In Situ Characterization of the Dynamic Gold–Support Interaction over Ceria Modified Eu3+. Influence of the Oxygen Vacancies on the CO Oxidation Reaction

ARTICLE *in* THE JOURNAL OF PHYSICAL CHEMISTRY C · JUNE 2010

Impact Factor: 4.77 · DOI: 10.1021/jp1013225

4 AUTHORS:

W. Yesid Hernández Enciso
Ghent University
28 PUBLICATIONS **332** CITATIONS
SEE PROFILE

Francisca Romero-Sarria
Universidad de Sevilla
53 PUBLICATIONS **785** CITATIONS
SEE PROFILE

Miguel Angel Centeno
Spanish National Research Council
201 PUBLICATIONS **3,277** CITATIONS
SEE PROFILE

Jose Antonio Odriozola
Universidad de Sevilla
292 PUBLICATIONS **4,347** CITATIONS
SEE PROFILE

In Situ Characterization of the Dynamic Gold−Support Interaction over Ceria Modified Eu^{3+}. Influence of the Oxygen Vacancies on the CO Oxidation Reaction

Willinton Y. Hernández,* Francisca Romero-Sarria, Miguel A. Centeno, and Jose A. Odriozola

Institute of Materials Science of Seville, Joint Center University of Seville−CSIC, Avda. Américo Vespucio 49, 41092 Seville, Spain

Received: February 11, 2010; Revised Manuscript Received: May 13, 2010

Gold-supported ceria and europium-doped ceria catalysts were prepared by the deposition−precipitation method. The influence of the pretreatment atmosphere and temperature on the concentration of oxygen vacancies and gold dispersion on the Au/CeEu(10) catalyst under actual reaction conditions was investigated by "in situ" X-ray diffraction and Raman analysis. By Raman spectroscopy, a preferential interaction of the gold with the support across the oxygen vacancies was established and correlated with the gold dispersion. The increase in the concentration of oxygen vacancies in the presence of hydrogen induces changes in the gold crystallite size by breaking-off and migration of gold nanoparticles toward the oxygen vacancies on the CeEu(10) support. The activity of the Au/CeEu(10) solid in the CO oxidation reaction was significantly improved when the catalyst was preactivated in a reducing atmosphere. This trend could be associated with the redispersion of gold together with the increase in the concentration of oxygen vacancies in the support.

1. Introduction

Highly disperse, Au-supported metal oxide catalysts are extremely active for oxidation reactions, in particular, for CO oxidation at low temperatures.[1−3] Several models have been proposed for explaining the activation of supported gold: from special chemical properties resulting from the limited size of the active gold particles (usually less than 10 nm), to the effects of metal−support interactions (i.e., charge transfer between the oxide and gold).[3−6] In principle, the active sites for the catalytic reactions could be located only on the supported Au particles or on the perimeter of the gold−oxide interface.[1,4,7−9]

The Au/support interface can be seen as a model of a metal−semiconductor or metal−insulator junction bearing unique size-dependent electronic properties, which could have an essential role in the origin of the catalytic activity.[10] The supports, generally being metal oxides, are divided in two categories: the reducible (Fe_2O_3, TiO_2, Co_2O_3, CeO_2) and the nonreducible supports (SiO_2, Al_2O_3, MgO). In the case of nonreducible metal oxides, the principal role of the support is limited to the stabilization of very small particles and/or particles with highly reactive gold sites or crystallite faces.[8] Otherwise, the reducible supports are consider as "active" in the reaction of CO oxidation because they are able to provide reactive species from their structure, either by oxygen mobility in the network of material or by oxygen adsorption from the gas phase.[11−13] In both cases, the presence of oxygen vacancies in the support is very important in the mechanism of reaction, together with their possible role as nucleation centers for the nanogold particles in gold catalysts.[14−16] Therefore, the presence of oxygen vacancies affects both the reactivity of the support and the gold dispersion on the material, modifying the electronic properties of the gold particles.

Ceria has been established as one of the most promising active supports used in redox catalytic applications, on one hand, due to its remarkable oxygen storage capacity and, on the other hand, by leading stabilization of small gold particles.[17] It is well-known that the addition of ions with oxidation state different from (4+) to ceria causes the formation of a defective fluorite structure with increased oxygen mobility and enhanced thermal stability properties.[18] So, doped ceria can be seen as a very interesting material, taking into account: (i) the enhanced catalytic properties of the support by the increase of the oxygen vacancies (oxygen mobility, reducibility) and (ii) the modification of the gold−support interaction by the presence of these punctual defects.

Several doped-ceria systems have been investigated for catalytic applications such as total oxidation of CO,[11,19−22] combustion of diesel soot,[23,24] preferential oxidation of CO in the presence of hydrogen (Prox),[25] total oxidation of propene,[26] and water−gas shift reactions.[27] In general, it is accepted that an increase in the number of oxygen vacancies on the material results in an enhancement of its catalytic properties, due to the presence of oxygen actively coming from the gas phase−support interaction and/or by the mobility of lattice oxygen during the catalytic reaction. More recently, several works have been focused in the use of doped-ceria systems as support for gold nanoparticles applied to different catalytic processes.[28−31] In the preferential oxidation of CO in the presence of hydrogen (Prox) reaction, the ability of Au/doped-ceria to tolerate the presence of CO_2 and H_2O in the feed is higher compared to that of Au/undoped-ceria, in special for supports doped with Zn and Sm.[28,32] For NO_x reduction by CO, an increase in the activity and selectivity toward N_2 is obtained using lanthanides as dopants of the ceria support.[29] Generally, these results are discussed as a function of the reducibility of the supports and the gold−support interfacial interaction across oxygen vacancies. The nature of the gold−oxygen vacancy interactions on CeO_2 surfaces have been studied by density functional theory calculations (DFT).[33−36] These works revealed that Au particles nucleate mainly on the oxygen vacancies in a reduced CeO_x surface, allowing the growth of small and well-dispersed clusters, which facilitate the reactivity of the catalyst. As expected, the Au−oxygen vacancy interaction promotes changes in the electronic environ-

* To whom correspondence should be addressed, willinton.yesid@icmse.csic.es.

10.1021/jp1013225
Published on Web 06/02/2010

ment of the gold because electron transfer between them is possible. Experimentally, this effect has been observed by means of infrared spectroscopy through the presence of a band at 2060 cm^{-1} assigned to CO absorbed on an $Au^{\delta-}$ site.[37] In the same way, a blue shift of the binding energy of the Au 4f level due to an electronic enrichment of gold has been reported by X-ray photoelectron spectroscopy (XPS) for gold catalysts supported on CeO_2 and $CeO_2-Al_2O_3$.[38] This effect was related to the presence of a higher amount of oxygen vacancies in the ceria−alumina support.

As we established previously,[11] the $Ce_{1-x}Eu_xO_{2-x/2}$ system presents a high number of surface oxygen vacancies, especially when the amount of dopant is around 10% (w/w). The resultant solid shows enhanced catalytic properties for the CO oxidation reaction. Similar conclusions have been recently reported for $Fe_2O_3-CeO_2$ composite catalyst[19] and $Ce_{1-x}Pr_xO_{2-\delta}$ solid solutions[22] in the same reaction. The goal of this work is studying the influence of the oxygen vacancies in the catalytic properties of gold−ceria catalyst in the CO oxidation reaction. For this purpose, a gold catalyst supported on 10% w/w $Eu_2O_3-CeO_2$ was prepared, characterized by in situ techniques (Raman and XRD), and tested in the CO oxidation reaction. The obtained results were compared with those of an Au/CeO_2 catalyst synthesized with the same procedure.

2. Experimental Methods

2.1. Preparation of the Samples. The preparation of $Ce_{1-x}Eu_xO_{2-x/2}$ solid solution containing 10 wt % has been described elsewhere.[11] The appropriate amounts of $Ce(NO_3)_3 \cdot 6H_2O$ (Alfa Aesar 99,5%) and $Eu(NO_3)_3 \cdot 6H_2O$ (Alfa Aesar 99,9%) were dissolved in distilled water to obtain a 0.1 M solution. Then the cationic solutions were precipitated by addition of ammonium hydroxide (30% w/w), at room temperature under continuous stirring. The precipitated gel was washed by filtration with distilled water and dried overnight at 100 °C. Finally, the sample was calcined at 300 °C for 2 h (10 °C/min).

Pure cerium oxide was also prepared for comparative purposes by adopting the same precipitation method.

The gold catalysts were prepared by the deposition−precipitation method (DP), first developed by Haruta et al.[1] The adequate amount of $HAuCl_4 \cdot 3H_2O$ (Alfa Aesar 99,9%) to obtain 1% (w/w) gold catalysts (metal base) was dissolved in distilled water to get a $\sim 6.0 \times 10^{-4}$ M gold solution. The pH of the gold solution was adjusted around 8 by addition of 0.1 M NaOH. The solution was heated to 70 °C, and then the support was added and kept under continuous stirring for 1 h. The obtained solids were washed several times with distilled water in order to remove the Cl^- and Na^+ ions and dried overnight at 100 °C. Finally, the catalysts were calcined at 300 °C for 2 h (10 °C/min).

2.2. Characterization. BET specific surface areas were measured by nitrogen adsorption at liquid nitrogen temperature in a Micromeritics ASAP 2000 apparatus. Before analysis, the samples were degassed 2 h at 150 °C in vacuum.

The chemical composition of the samples was determined by X-ray fluorescence spectrometry (XRF) in a Panalytical AXIOS PW4400 sequential spectrophotometer with a rhodium tube as the source of radiation.

X-ray diffraction (XRD) analysis was performed on a Siemens D 500 diffractometer. Diffraction patterns were recorded using Cu Kα radiation (40 mA, 40 kV) over a 2θ range of 10°−90° and a position-sensitive detector using a step size of 0.05° and a step time of 1 s. The reflection from the (111) plane was used for the determination of the average crystallite size, D, calculated from the Scherrer equation.

Temperature programmed reduction (TPR) of the catalysts was carried out using 5% hydrogen in Ar at 50 $mL \cdot min^{-1}$. About 50 mg of catalyst was loaded in a U-shaped quartz reactor and heated from room temperature to 900 at 10 $°C \cdot min^{-1}$. The effluent gases were analyzed by means of a TCD detector. Hydrogen consumption was determined upon calibration of the system with CuO (Strem Chemicals, 99.999% Cu). The Raman spectra were recorded in a dispersive Horiva Jobin Yvon LabRam HR800 microscope, with a 20 mW He−Ne green laser (532.14 nm), without filter, and with a 600 $g \cdot mm^{-1}$ grating. The microscope used a 20× objective and a confocal pinhole of 150 μm. The Raman spectrometer is calibrated using a silicon wafer. The "in situ" Raman measurements of the samples were performed using a Linkam CCR1000 cell, coupled to the linked Raman equipment. The cell allows the use of controlled atmosphere and temperature. The sample was inserted in the cell and heated at 400 °C for 15 min under synthetic air (S.A.: 21% O_2 and 79% N_2) atmosphere with a heating rate of 20 °C/min. After that the samples were cooled down to room temperature, an adequate atmosphere was introduced (N_2, H_2, or synthetic air), and the samples were heated up to 400 °C again, with a spectrum taken each 50 °C after 15 min stabilization.

Mapping Analysis. Spectra were collected using the Labspec mapping software for the FT-Raman instrument (Jobin Yvon) in conjunction with a motorized XY microscope stage for point by point or laser scanning imaging. An XY list was generated, keeping the Y coordinate at (0,0), so that mapping would proceed along the X axis. Increments of 10 μm were used, with 10 positions in total. After the first spectrum was aquired, the sample stage is moved automatically to the next coordinate required.

2.3. Catalytic Activity. The CO oxidation tests were carried out in a conventional continuous flow U-shaped glass reactor (7 mm i.d.) under atmospheric pressure. The sample (80 mg, 100 $\mu m < \phi < 200$ μm) was placed between glass wool. A thermocouple in contact with the sample assures the right measure of the temperature. The feed mixtures were prepared using mass flow controllers (Bronkhorst). The reaction was followed by mass spectrometry, using a Balzers Thermostar benchtop mass spectrometer controlled by the software Balzers Quadstar 422 with capabilities for quantitative analysis. The light-off curves of CO oxidation (400 °C, 5 °C/min) were obtained with a mixture of 3.4% CO (Air Liquide, 99.997% pure, <3 ppm H_2O) and 21% O_2 (Air Liquide, 99.999% pure, <3 ppm H_2O) balanced by He (Air Liquide, 99.999% pure, <3 ppm H_2O) at a total flow rate of 42 mL/min. Before all catalytic measurements, the samples were preactivated "in situ" in a mixture of 21% O_2 in He (30 mL/min, at 300 °C for 1 h) or 100% H_2 (10 mL/min, at 300 °C for 1 h), followed by cooling to room temperature in activation atmosphere.[39]

3. Results and Discussion

3.1. Chemical Analysis and Surface Area. Table 1 shows the code, gold content, textural properties, and average crystallite size (support and gold metallic phase) of the prepared solids. The gold loading in the synthesized catalysts is approximately the same as the target value indicating no appreciable loss of metal during the precipitation and washing procedures. In fact, the amount of gold seems to be higher than the nominal value employed for the DP process. This feature could be correlated with the relatively high heterogeneity of the gold distribution

TABLE 1: Gold Content, Textural Properties and Crystallite Sizes of the Studied Supports and Gold Catalysts

code	Au content (% w/w)	S_{BET} (m^2/g)	pore volume (cm^3/g)	CeO_2 crystallite size (nm)	Au crystallite size (nm)
CeO_2		69	0.141	15	
CeEu(10)		84	0.143	13	
Au/CeO_2	1.3	79	0.149	14	20
Au/CeEu(10)	1.1	86	0.144	12	16

on the catalysts, further observed and discussed from Raman spectroscopy analysis. As has been reported,[11] the higher S_{BET} area of the europium-doped support compared to bare CeO_2 results from the formation of a CeO_2/Eu_2O_3 solid solution, which hinders the sinterization during the calcination step.

BET surface area and pore volume of the gold catalysts do not show significant variation compared to those of the supports. Only Au/CeO_2 solid presents a little increase in this value (~12%) without modification in their pore volume (Table 1).

3.2. X-ray Diffraction. The XRD patterns of the studied solids are presented in Figure 1. The crystalline structure and the average size of the crystalline domain of the CeO_2 and CeEu(10) supports are maintained in the gold samples (Table 1). Moreover, reflections at 38.5 and 44.8°2θ, corresponding to (111) and (200) planes of metallic gold (JCPDS card no. 04-0784), are observed in these materials. The average gold crystallite size, calculated by Scherrer equation, was 20 and 16 nm for the Au/CeO_2 and Au/CeEu(10) catalysts, respectively, table 1.

3.3. H_2-TPR Analysis. The reducibility of CeO_2 and CeEu(10) supports was examined by H_2-TPR analysis, and the reduction patterns are depicted in Figure 2. The temperatures of the peak maxima and their respective hydrogen consumption are given in Table 2. As reported in literature, based ceria supports are characterized by a low temperature peak, below 600 °C, attributed to reduction of the surface oxygen species (LT peak), and a high temperature one, centered between 700 and 800 °C, due to bulk oxygen species (HT peak).[32,40] For the CeEu(10) sample, the temperature of the maximum LT peak slightly shifts to higher temperatures than that of bare CeO_2, with a higher hydrogen consumption also. Even being the CeEu(10) solid reduced at higher temperature than pure CeO_2, its higher hydrogen consumption during the surface reduction step could be related with the ability of the oxygen vacancies to adsorb

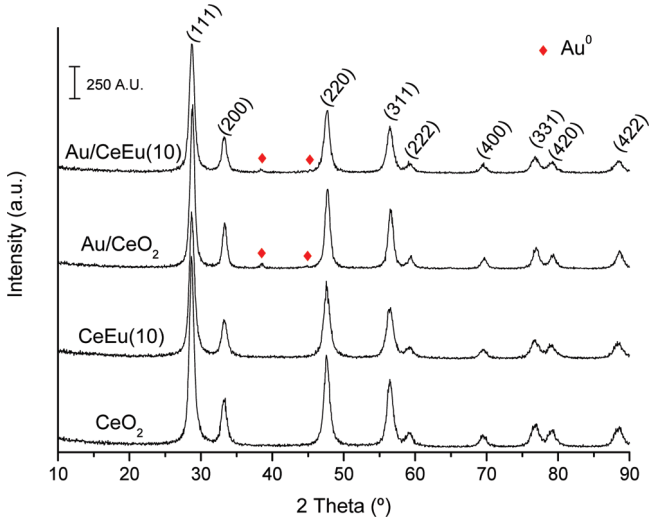

Figure 1. X-ray diffraction patterns of the studied supports and gold catalysts.

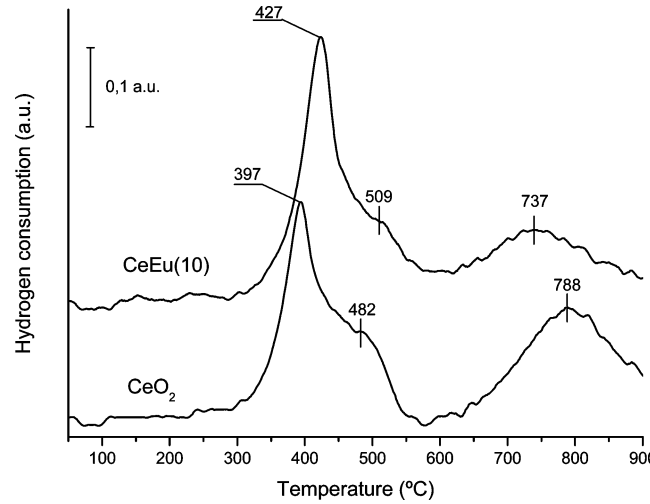

Figure 2. H_2-TPR profiles of the studied supports.

TABLE 2: TPR Peak Maxima and H_2 Uptake of Synthesized Supports and Gold Catalysts

	peak position (°C)		H_2 consumption (μmol/g of $CeO_2 \cdot m^2$)	
catalyst	T_{LT}	T_{HT}	η_{LT}	η_{HT}
CeO_2	397; 482	788	8.28	6.23
CeEu(10)	427; 509	737	9.53	6.37
Au/CeO_2	164	790	8.79	8.47
Au/CeEu(10)	153; 183	738	12.27	5.12

and dissociate H_2,[41,42] taking into account the increased concentration of these punctual defects in this solid.[11] Thus, a higher concentration of oxygen vacancies improves the surface and subsurface reaction with the hydrogen. On the other hand, for the CeEu(10) sample, the temperature of maximum HT peak is strongly decreased in comparison with the CeO_2 solid (737 to 788 °C respectively). This trend can be associated with an increase in the reducibility of the bulk material by enhancing of the oxygen mobility, associated to the presence of a high concentration of oxygen vacancies. Because the hydrogen consumption was normalized considering the surface area of the supports, the value obtained for the HT peaks appear to be the same for CeO_2 and CeEu(10) materials (Table 2), in a good agreement with a bulk reduction process.

In the case of the reduction profiles of Au/CeO_2 and Au/CeEu(10) catalysts (see Figure 3), the HT peak position remains unchanged compared with the respective supports, whereas the LT peak shifts to low temperature as an indication of the increased surface oxygen reducibility.[43] The LT peak of Au/CeO_2 catalyst exhibits a slightly asymmetric shape centered at T_{max} = 164 °C while Au/CeEu(10) sample shows two overlapping peaks with maximum at T_{max} = 153 and 183 °C. In both cases, the LT peak is characterized by a high-temperature tail which can be associated with a complex reduction process due to the heterogeneous ceria surface. In fact, the differentiation of two overlapping peaks in the Au/CeEu(10) catalyst, one of them at lower temperature than that observed for Au/CeO_2 sample, suggests that the surface oxygen reducibility may be affected (in a different way) by the interaction between the reducible species with the oxygen vacancies in a higher concentration in the CeEu(10) support, previously demonstrated.[11] Thus, the surface reduction on the Au/CeEu(10) catalyst results intensified in a phased reduction process by the gold−oxygen vacancy interaction and the increased oxygen mobility in the bulk material.

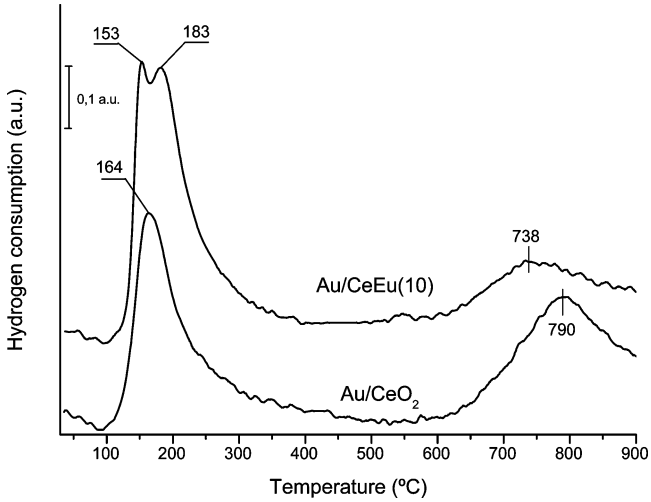

Figure 3. H_2-TPR profiles of the studied gold catalysts.

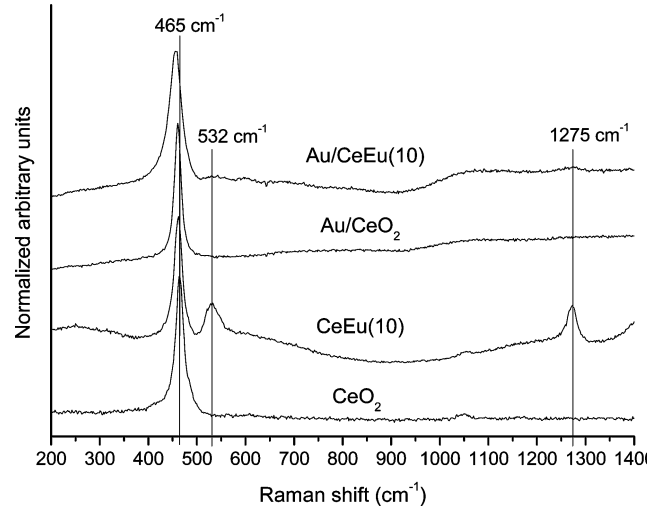

Figure 4. Raman spectra of the initial supports and gold containing catalysts.

A quantitative comparison of the reduction processes of the studied gold catalyst is given in Table 2. Previous studies of gold deposited on hardly reducible titania and zirconia supports[44,45] have shown that the reduction process of the oxidized gold species occurs in the range temperature of the observed LT reduction peak. However, in the present case (~1 wt % Au on reducible support) the hydrogen consumption by the oxidized gold is negligible compared to that needed for the surface reduction of ceria. For both catalysts, the hydrogen consumption of the LT reduction peak is higher than that of the HT one, which could be indicative of the high surface reducibility of ceria improved by the presence of gold nanoparticles.[32,40] On the other hand, for the Au/CeEu(10) catalyst, the hydrogen consumption for the LT reduction peak is higher than that of the Au/CeO_2 sample. Similar results have been reported for gold-based ceria catalysts doped with rare earth metals (Sm^{3+}, La^{3+}, and Gd^{3+})[30,32] and correlated with the increase in the number of oxygen vacancies by the presence of the dopant cation, enhancing the oxygen mobility in the support and, consequently, the reduction process. In fact, the decreased hydrogen consumption of the HT peak in Au/CeEu(10) catalyst compared with Au/CeO_2 shows the intensified surface reduction process in this catalyst, causing that part of the reducible species from the bulk reduces now as a surface process.

So, from qualitative and quantitative TPR analyses of the catalysts studied in this work, it is clear that the enhanced reducibility properties on the Au/CeEu(10) sample correlated principally by the increased concentration of oxygen vacancies induced by the presence of Eu^{3+} in the support. This feature should influence the gold properties of the catalysts and their activity in the catalytic oxidation of carbon monoxide, taking into account the reported influence of these punctual defects in the reaction mechanism.[11−13]

3.4. Raman Spectroscopy. Figure 4 shows the Raman spectra of the supports and the gold containing catalysts. The main band of CeO_2 (465 cm^{-1}), corresponding to the oxygen breathing vibrations around Ce^{4+} ($F_{2\,g}$ mode),[46] dominates the Raman spectra of all solids. For the CeEu(10) support, there are two additional bands around 532 and 1275 cm^{-1} which have been attributed to the formation of oxygen vacancies in the $Ce_{1-x}Eu_xO_{2-x/2}$ solid solution.[11] After gold deposition, no important differences can be seen on the vibrational mode of ceria. Nevertheless, the bands ascribed to oxygen vacancies in the CeEu(10) support are strongly decreased, almost disappearing, when gold is deposited. This result can be interpreted as a direct gold−support interaction across the oxygen vacancies present in the CeEu(10) material, by means of a "filling effect" of the oxygen defective sites by the gold nanoparticles. This type of interaction has been widely documented by both theoretical and experimental studies, finding that the gold−oxygen vacancy surface interaction is energetically favored and modifies the electronic properties of the deposited metal.[14−16,33−38,47] So, when the support is put in contact with the gold solution during the deposition−precipitation process, an individual Au atom can occupy an oxygen vacancy, acting as the nucleation site for the growth of a gold cluster. Thus, the vibrational mode in the Raman spectra generated by the presence of these punctual defects in the network of ceria disappears as a result of the "fill" of the vacancy. This effect has been described as "metal nesting" by Sanchez et al.[48] in their oxygen vacancy model in strong metal−support interaction for Rh, Ir, Pd, and Pt atoms in contact with fluorite and cassiterite structures. In fact, the smaller gold particle size in the Au/CeEu(10) sample (Table 1) compared to that of the Au/CeO_2 material, could be related with a higher gold dispersion induced by the presence of a higher concentration of oxygen vacancies in the CeEu(10) support and their direct interaction with gold.

Therefore, from the obtained results in this work, additional evidence of the interaction of gold nanoparticles with the oxygen vacancies of ceria-doped supports is offered using Raman spectroscopy. The specific nature of this interaction is beyond the scope of this study. However, by "in situ" Raman analysis it is possible to have a first idea of their stability in function of the reaction atmosphere and temperature and to correlate the obtained results with the catalytic activity in the reaction of CO oxidation.

Before starting the "in situ" Raman studies, the surface homogeneity of the considered samples (CeEu(10) support and Au/CeEu(10) catalyst) was evaluated by point by point mapping Raman analysis of a 100 μm length zone. The spectra obtained for the CeEu(10) support and Au/CeEu(10) catalyst are presented in Figure 5 and Figure 6, respectively, in a stack profile.

The ratio between the areas of the 532 cm^{-1} (A_{532}) and 465 cm^{-1} (A_{465}) Raman bands is a measurement of the number of oxygen vacancies in the solid solution, in such a way that the higher the number of oxygen vacancies, the higher the A_{532}/A_{465} value.[11,19,20,22,49] For this material, the ratio between the 465 cm^{-1} Raman band due to CeO_2 structure and that at 532 cm^{-1}, attributed to oxygen vacancies, is constant across the analyzed region (see Figure 7). This result indicates a good homogeneity

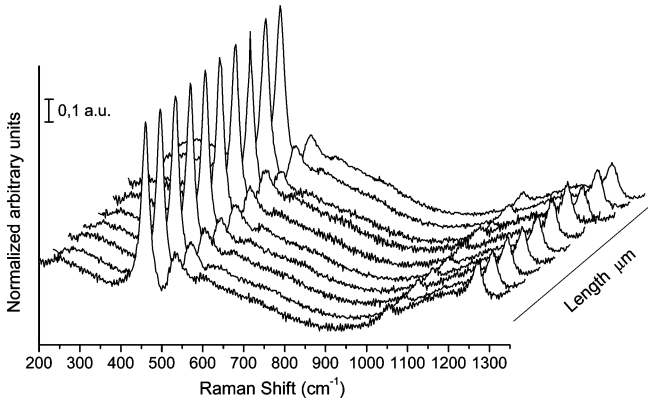

Figure 5. Raman mapping analysis of CeEu(10) support as a fucntion of length.

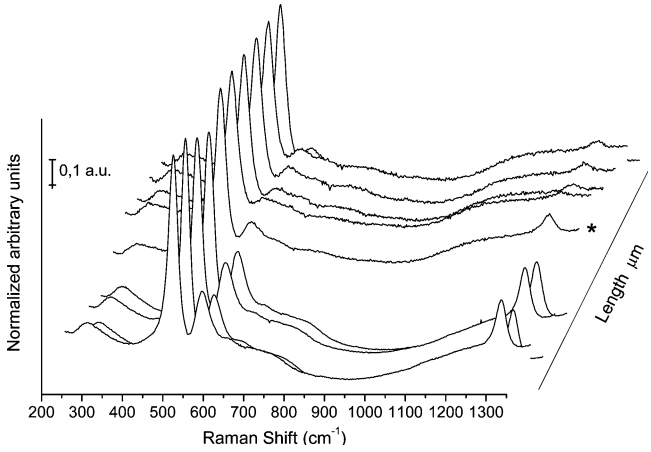

Figure 6. Raman mapping analysis of Au/CeEu(10) catalyst as a fucntion of length.

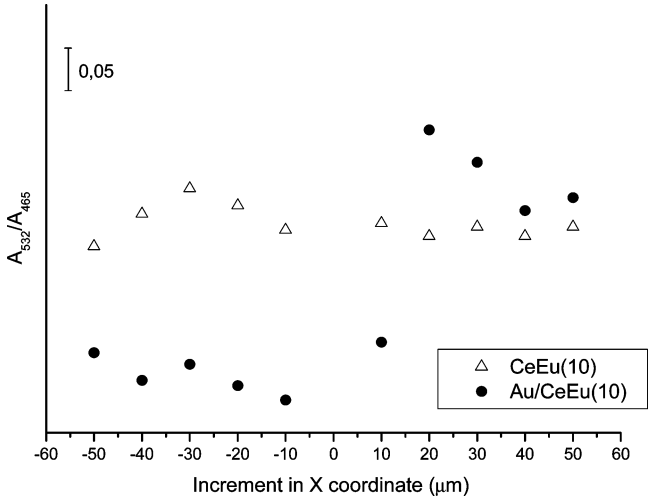

Figure 7. Relationship between A_{532}/A_{465} and length from Raman mapping analysis obtained for CeEu(10) support and Au/CeEu(10) catalyst.

of the surface sample composition for the CeEu(10) support since this ratio can be influenced by a lot of different factors such as europium content, ceria particle size, change in the optical absorption properties, presence of defects, etc.[11,49] However, the spectra obtained from the mapping Raman analysis on the Au/CeEu(10) catalysts shows a wide-ranging ratio of A_{532}/A_{465} values (see Figure 7). This observation points to the existence of an irregular distribution in the number of oxygen vacancies in the solid, suggesting the inhomogeneous distribution of gold nanoparticles on the surface support. In fact, the images obtained through the microscope of the Raman apparatus show different contrasted areas. Darker areas present a very low A_{532}/A_{465} ratio, providing evidence of a low amount of oxygen vacancies in them. From this, a high concentration of gold could be envisaged to exist in this region, as was discussed early, which could be responsible of the darkness of the image. In good agreement, clearer areas show a similar A_{532}/A_{465} ratio to that of the support, pointing out the low amount of gold on them. On the basis of the above observations, a medium dark area of the sample was chosen to perform the "in situ" Raman analysis in order to be able follow the changes in the number of oxygen vacancies of the solid with different atmospheres (N_2, H_2, and synthetic air) and temperature, in a region where gold is also present, in such a way that the gold−oxygen vacancy interactions can also be evaluated. A representative Raman spectrum of this area is marked with an asterisk in Figure 6.

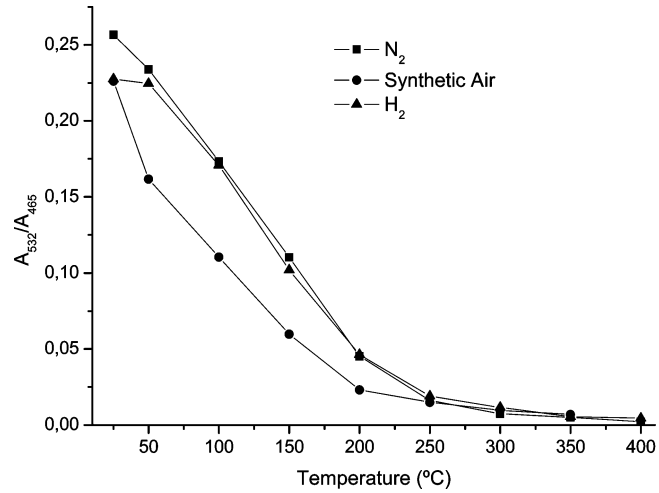

Figure 8. Relationship between A_{532}/A_{465} and temperature under different atmospheres for CeEu(10) support.

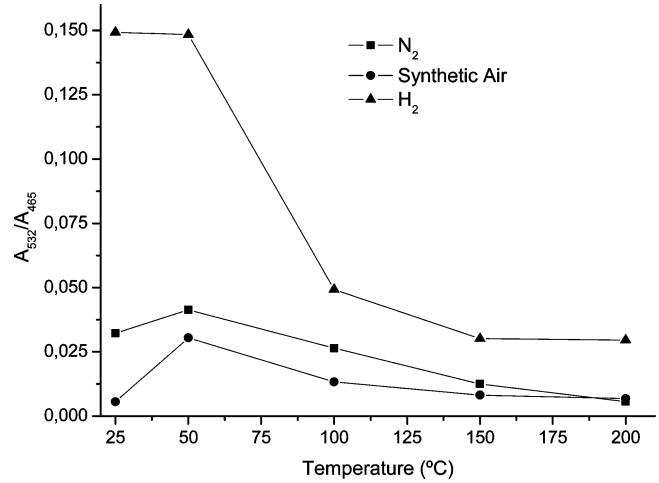

Figure 9. Relationship between A_{532}/A_{465} and temperature under different atmospheres for Au/CeEu(10) catalyst.

Figure 8 and Figure 9 show the evolution of the A_{532}/A_{465} ratio with temperature under N_2, H_2, and synthetic air for CeEu(10) and Au/CeEu(10) catalysts. For the CeEu(10) support, the A_{532}/A_{465} value decreased with increasing temperature in all atmospheres. The same tendency has been reported for a $Ce_{0.9}Pr_{0.1}O_{2-\delta}$ solid solution in the presence of O_2, He, and H_2 gases using a 514 nm excitation laser, being associated to changes in the Pr surface content by redistribution of Pr during

the heating taking into account that, with this excitation laser line, only surface information was provided.[49] In the same way, in a previous work, a similar trend was established with the increase of Eu content in $Ce_{1-x}Eu_xO_{2-x/2}$ solid solutions and was rationalized by the conjunction of positive effects due to the presence of oxygen vacancies with negative ones due to changes in the europium surface distribution or changes in the penetration depth of the Raman radiation.[11] So, in this case, a negative effect of the temperature on the oxygen vacancies concentration is clear, independently of the used atmosphere, and could be correlated with the migration of europium cations in the solid solution by thermal effects since we can attend an increment in the number of oxygen vacancies with the temperature, especially under reducer atmosphere. On the other hand, although the effect of the nature of the atmosphere in the A_{532}/A_{465} value for the CeEu(10) support is very similar, some differences can be seen principally when S.A. is employed. In this atmosphere, the A_{532}/A_{465} ratio presents lower values than those obtained in N_2 and H_2, for temperatures between 50 and 200 °C. Hence, the concentration of oxygen vacancies is more affected when oxygen is in the atmosphere of treatment. This observation agrees with the possibility to generate more oxygen vacancies in the support with temperature, depending of the atmosphere. In this way, when S.A. is used, the presence of gaseous oxygen difficult two principal processes to generate additional oxygen vacancies: (i) the kinetics of depletion of oxygen from the structure by the effect of temperature and (ii) the reduction of Ce^{4+} to Ce^{3+} in the ceria structure. When hydrogen or nitrogen is present, these two processes are allowed.

For the Au/CeEu(10) gold catalyst (see Figure 9), the evolution and variation of the A_{532}/A_{465} values are different in function of the temperature and atmosphere compared with that of the support. As was explained before, the A_{532}/A_{465} values are lower than those obtained from the CeEu(10) support, since the presence of gold reduces significantly the signal associated to the presence of oxygen vacancies. For this catalyst, the concentration of oxygen vacancies is always higher in the presence of H_2 then in N_2 and finally S.A. With increase of the temperature, the variation of the A_{532}/A_{465} ratio is lower than that of the support, especially in the presence of N_2 and S.A., with a slight increase in this value above 50 °C. Because the information obtained with the laser employed for this study is principally from the surface of the material,[11] the presence of gold could make the analysis of the surface modification induced by the thermal treatment discussed for the CeEu(10) support difficult. Nonetheless, the presence of hydrogen improves the concentration and stability of the oxygen vacancies compared with the other gases used here. In the same way that was discussed for CeEu(10) support, the presence of H_2 provides a reducing atmosphere for the gold catalyst, facilitating the reduction of Ce^{4+} to Ce^{3+} to generate more oxygen vacancies. In addition, the reducibility of the support can be increased by the presence of both Eu^{3+} dopant cation and Au, as was established by H_2-TPR analysis. It is wellknow that in analogy with other noble metals, metallic gold could activate the hydrogen with subsequent spillover on the support and promotion of the ceria reduction at lower temperatures.[50] It has also been suggested that the surface oxygen reducibility may be enhanced through a lattice substitution effect, leading to the formation of oxygen vacancies and, thus, increasing the oxygen mobility and reducibility.[43] Along with the increase in the number of oxygen vacancies in the support, changes in the distribution of gold on the surface catalyst are possible by the diminishing of the gold−support interaction energy across

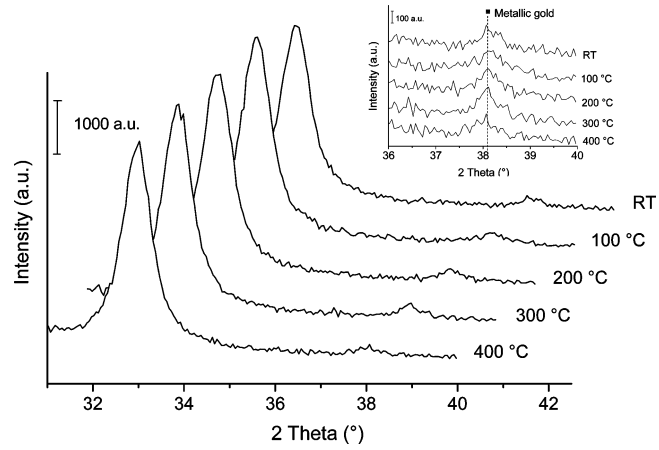

Figure 10. XRD patterns at increasing temperatures in the presence of synthetic air for Au/CeEu(10) catalyst. Insert shows the enlarged gold metallic phase area.

the oxygen vacancies. In Au/CeO_2 catalyst, Romero-Sarria et al.[5] have established by "in situ" DRIFTS studies that a deep reduction of the surface (oxygen vacancy creation) provokes changes of the gold dispersion and migration of oxygen atoms from the bulk to the surface, generating oxidized species. This result was also confirmed by XRD analysis of the catalyst before the CO oxidation reaction, where a decrease in the intensity of all metallic gold diffraction peaks was interpreted as a diminishing in the gold crystallite and particle sizes. In the same way, gold redispersion can be also influenced by the hydroxylation degree of the surface. In this sense, it has been reported that a competition between the hydroxyl groups and the gold particles for the oxygen vacancies exists.[33,51] During the catalytic test, the increase in the temperature reaction provokes the surface dehydroxilation, liberating the vacancy and allowing the gold−vacancy interaction driving to the gold redispersion. This redispersion of gold during reaction conditions has also been established by Goguet et al.[52] over gold catalysts supported on carbon. These authors proved by XRD, TEM, and EXAFS analysis the modification of the gold particle size during the first period of reaction (carbonylation of methanol to methyl acetate in presence of methyl iodide) and correlated an induction period of the catalysts with the necessary time to reach the adequate gold particle size to have the highest activity in the reaction.

3.5. "In Situ" X-ray Diffraction. "In situ" XRD analysis was employed to establish the possible changes in the gold particle size as a function of the atmosphere (oxidizing or reducing) and temperature (from room temperature to 400 °C) on the Au/CeEu(10) catalyst. The effect of synthetic air or hydrogen was evaluated in the range of 30−40 2θ° to have an idea of the modification of (111) reflection from the support, together with the modification of (111) reflection coming from the gold metallic phase. The XRD patterns obtained from this study are presented in the Figure 10 and Figure 11 for synthetic air and hydrogen atmospheres respectively.

In presence of an oxidizing atmosphere (see Figure 10), the reflection associated to the presence of gold metallic phase (about 38.5°2θ) is not strongly modified with the increase of temperature. However, when S.A. is replaced by hydrogen (see Figure 11), an immediate change in the intensity of this XRD peak is produced. The virtual disappearance of the gold's XRD pattern is evident in the entire range of analyzed temperatures. This result indicates an increase in the gold dispersion by breaking off the original gold crystals, related with the surface reduction, by hydrogen. Similar observations have been reported

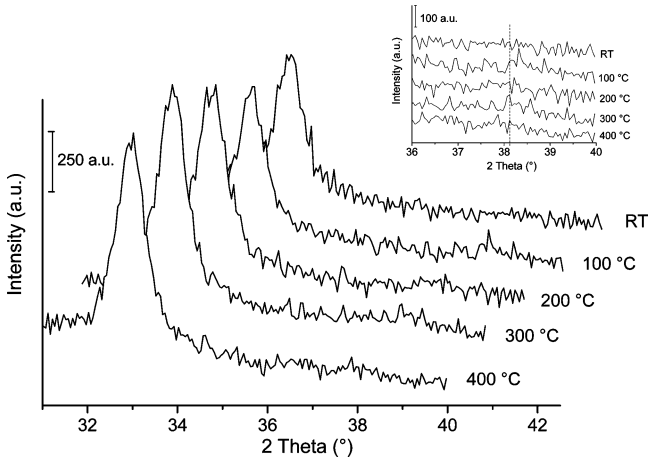

Figure 11. XRD patterns at increasing temperatures in presence of hydrogen for Au/CeEu(10) catalyst. Insert shows the enlarged gold metallic phase area.

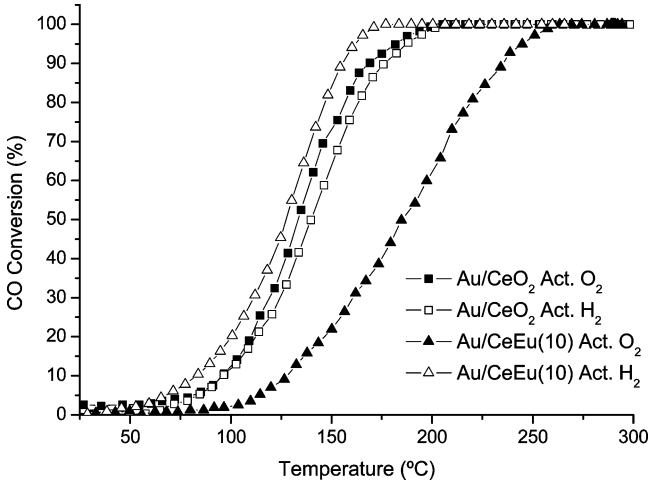

Figure 12. CO conversion of the studied gold catalyst, preactivated in different atmospheres.

in a previous work for Au/CeO_2 in reaction conditions by the reducing effect of the CO[5] and it has also been observed by Goguet et al. by XRD analysis after carbonylation of methanol reaction on gold catalysts supported on carbon.[52] Additionally, when the atmosphere is changed again to S.A., diffraction peaks due to metallic gold reappear, recovering its position and intensity, indicating the reversibility of the gold redispersion process. Thus, from the "in situ" techniques employed in this work, clear evidence of the dynamic gold−support interaction on a gold catalyst supported on ceria doped by Eu^{3+} is reported. Under a hydrogen atmosphere, an increase in the concentration of oxygen vacancies (inherent to the reducibility of the material itself) is accompanied by an increase in the gold dispersion on the catalyst. On the other hand, the presence of oxygen provokes the oxygen vacancies healing and a modification of the gold particle size is observed. This last feature could be associated to the hierarchy of the gold−gold (metallic and/or ionic species) interaction in front of the interaction of the metallic phase with the support when the energetically favorable gold−support conjunction across of the oxygen vacancies disappears. All these changes occur even at room temperature over the Au/CeEu(10) catalyst.

3.6. Catalytic Activity. Total Oxidation of CO (TOX). Figure 12 shows the CO conversion as a function of the temperature for Au/CeO_2 and Au/CeEu(10) catalysts using an oxidative or reductive atmospheres for the pretreatment of the

TABLE 3: Catalytic Evaluation Parameters in the CO Oxidation Reaction of the Studied Catalysts

code	activ atmosphere	T_{50} (°C)	ΔT_{50} (°C)	T_{100} (°C)	ΔT_{100} (°C)
Au/CeO_2	O_2	134		196	
	H_2	140	6	200	4
Au/CeEu(10)	O_2	185		252	
	H_2	128	57	170	82

catalyst just before the reaction. When the catalysts were activated in the presence of oxygen, Au/CeO_2 solid presents better catalytic activity than Au/CeEu(10) catalyst, reaching 100% CO conversion at lower temperature. In our previous work about the characterization and catalytic evaluation of CeO_2/Eu_2O_3 mixed oxides,[11] we established that the formation of a $Ce_{1-x}Eu_xO_{2-x/2}$ solid solution implies an increase in the number of oxygen vacancies in the material. In the same way, a direct correlation was found between the concentration of these punctual defects and the catalytic activity of the support in the reaction of CO oxidation. However, the gold-supported catalysts do not follow the same tendency, the Au/CeEu(10) material being less active than the Au/CeO_2 despite having a similar gold particle size and structural and textural properties. Taking into account the evidence of the gold−oxygen vacancies interaction in the Au/CeEu(10) catalyst obtained by Raman spectroscopy analysis, two principal possibilities can be considered to explain this lower activity. The first one is the lost of actives sites from the support (oxygen vacancies) by the presence of gold species interacting with the surface material. In this sense, the activity of the support by itself is decreased in front that of the bare CeO_2. Similar results have been obtained for the room temperature CO oxidation on Au_n/TiO_2 solids prepared by size-selected deposition on single crystal rutile $TiO_2(110)$[53] for which, near-zero CO oxidation activity was found by a blocking effect of all vacancy sites by Au^+ deposition on the punctual defects. The second possibility to explain the low activity of the Au/CeEu(10) catalyst is the possible electronic change induced on the gold particles by the direct interaction with the surface oxygen vacancies in the support. In general, the vacancies are electron rich sites where a vacancy-bound Au will trend to have an increased electron density. However, the consensus on the role of gold charge in catalysis is not unanimous. For example, in some studies for identification of active places for the water−gas shift reaction (WGS), it has been established for Au/CeO_2 catalysts the direct participation of gold nanoparticles in contact with oxygen vacancies, which implies the presence of $Au^{\delta-}$ species.[36,37,54] Moreover, the CO bonding to a gold atom complexed to a vacancy has been proved to be weak by DFT calculations, CO-TPD experiments, and XPS technique.[55−57] In these works, these results have been explained by the transference of negative charge from the vacancy to the Au atoms, weakening the σ component of the CO−Au bond. In some cases this tendency is also dependent on the gold cluster size.[57] In this sense, for the Au/CeEu(10) catalyst, the weak adsorption of CO would imply a low reactivity in the reaction of total oxidation of CO, taking into account the role of gold as active site for the CO adsorption, together with the participation of the support to provide oxygen actives species during reaction.

On the other hand, when Au/CeO_2 and Au/CeEu(10) catalysts are preactivated in the presence of hydrogen, the activity of Au/CeEu(10) sample is strongly enhanced compared with that of Au/CeO_2 (see Figure 12). With the aim to express this result quantitatively, Table 3 presents the T_{50} and T_{100} values, which correspond to the temperatures at which the catalyst gets 50 and 100% of CO conversion, respectively. While for the Au/

CeO_2 solid the differences in the T_{50} and T_{100} values (ΔT_{50} and ΔT_{100}) between both activation atmospheres are very small (6 and 4 °C, respectively), for the Au/CeEu(10) catalyst these differences are very high, decreasing ΔT_{50} and ΔT_{100} about 57 and 82 °C, respectively, when activated in reducing atmosphere. So, after these reductive conditions of pretreatment, the gold catalyst supported on CeEu(10) material presents better catalytic properties than that of the Au/CeO_2 in the total oxidation of CO. Therefore, as was discussed from "in situ" Raman studies (section 3.4), the strong improvement of the Au/CeEu(10) catalyst by pretreatment in reductive atmosphere could be related with an increase in the oxygen vacancy concentration and an enhancement of the oxygen mobility together with the redistribution and/or redispersion of the gold particles on the surface support, as was established by "in situ" XRD (section 3.5). Dominguez et al.[12] reported high conversion of CO at room temperature for gold catalysts supported on calcium hydroxyapatite, as a result of the generation of structural vacancies by interaction of carbon monoxide with the solid, provoking the formation of peroxide species in the presence of gaseous oxygen. Likewise, Widmann et al.,[58] by quantitative temporal analysis of products, correlated the improved catalytic activity of the Au/CeO_2 catalyst in the CO oxidation reaction with the removal of about 7% of the surface oxygen by a reducing pretreatment.

In this way, the presence of Eu^{3+} in the gold ceria catalyst formulation facilitates the reduction of Ce^{4+} to Ce^{3+} increasing the oxygen vacancies concentration in a reductive atmosphere and enables enhancement of the catalytic properties of the material by improving the activity of the support itself, together with a better redispersion of the gold particles.

4. Conclusions

The results present in this work show that the increased concentration of oxygen vacancies in europium-doped ceria support promotes the interaction of the gold nanoparticles with the material surface across these punctual defects. By in situ XRD and Raman analysis, changes in the concentration of oxygen vacancies and gold dispersion depending of the employed atmosphere and temperature studied were established. A reducing atmosphere provokes an increase in the concentration of oxygen vacancies with the subsequent redispersion/redistribution of gold on the CeEu(10) support and, in a reversible way, when synthetic air is present. This gold−oxygen vacancy dynamic interaction affects the reactivity of the catalyst in the CO oxidation reaction. For Au/CeEu(10) catalyst, a pretreatment in hydrogen before of the reaction enhances its catalytic performances, which can be associated with the increase in the concentration of oxygen vacancies along with the redispersion of gold on the surface material. These results show the importance of the presence of oxygen vacancies in the support during the CO oxidation reaction over gold catalyst in two ways: (a) the improved catalytic activity of the support coming from the participation of the oxygen vacancies in the mechanism reaction, and (b) their participation as nucleation centers for the gold nanoparticles, modifying the dispersion of the metallic phase in the catalyst.

Acknowledgment. The financial support for this work has been obtained from Junta de Andalucía and Spanish Ministerio de Ciencia e Innovación (ENE2009-14522-C05-01), cofinanced by FEDER funds from European Union. F. Romero-Sarria thanks the Spanish MEC for her contract (Ramon y Cajal Programme). W. Y. Hernández thanks the AlBan program for the fellowship awarded (E06D101739CO).

References and Notes

(1) Haruta, M. *Catal. Today* **1997**, *36*, 153.
(2) Centeno, M. A.; Hidalgo, M. C.; Dominguez, M. I.; Navio, J. A.; Odriozola, J. A. *Catal. Lett.* **2008**, *123*, 198.
(3) Centeno, M. A.; Carrizosa, I.; Odriozola, J. A. *Appl. Catal., A* **2003**, *246*, 365.
(4) Centeno, M. A.; Portales, C.; Carrizosa, I.; Odriozola, J. A. *Catal. Lett.* **2005**, *102*, 289.
(5) Romero-Sarria, F.; Martinez, L. M.; Centeno, M. A.; Odriozola, J. A. *J. Phys. Chem. C.* **2007**, *111*, 14469.
(6) Vijay, A.; Mills, G.; Metiu, H. *J. Chem. Phys.* **2003**, *118*, 6536.
(7) Molina, L. M.; Hammer, B. *Appl. Catal., A* **2005**, *291*, 21.
(8) Schubert, M.; Hackenberg, S.; van Veen, A. C.; Muhler, M.; Plzak, V.; Behm, R. J. *J. Catal.* **2001**, *197*, 113.
(9) Avellaneda, R. S.; Ivanova, S.; Sanz, O.; Romero-Sarria, F.; Centeno, M. A.; Odriozola, J. A. *Appl. Catal., B* **2009**, *93*, 140.
(10) Sandoval, A.; Gómez-Cortés, A.; Zanella, R.; Díaz, G.; Saniger, J. M. *J. Mol. Catal. A* **2007**, *278*, 200.
(11) Hernández, W. Y.; Centeno, M. A.; Romero-Sarria, F.; Odriozola, J. A. *J. Phys. Chem. C* **2009**, *113*, 5629.
(12) Dominguez, M. I.; Romero-Sarria, F.; Centeno, M. A.; Odriozola, J. A. *Appl. Catal., B* **2009**, *87*, 245.
(13) Liu, H.; Kozlov, A. I.; Kozlova, A. P.; Shido, T.; Iwasawa, Y. *Phys. Chem. Chem. Phys.* **1999**, *1*, 2851.
(14) Wahlström, E.; Lopez, N.; Schaub, R.; Thostrup, P.; Rønnau, A.; Africh, C.; Lægsgaard, E.; Nørskov, J. K.; Besenbacher, F. *Phys. Rev. Lett.* **2003**, *90*, 026101.
(15) Lopez, N.; Nørskov, J. K. *Surf. Sci.* **2002**, *515*, 175.
(16) Wang, Y.; Hwang, G. S. *Surf. Sci.* **2003**, *542*, 72.
(17) Centeno, M. A.; Paulis, M.; Montes, M.; Odriozola, J. A. *Appl. Catal., A* **2002**, *234*, 65.
(18) Trovarelli, A. *Catal. Rev. Sci. Eng.* **1996**, *38*, 439.
(19) Bao, H.; Chen, X.; Fang, J.; Jiang, Z.; Huang, W. *Catal. Lett.* **2008**, *125*, 160.
(20) Pu, Z. Y.; Liu, X. S.; Jia, A. P.; Xie, Y. L.; Lu, J. Q.; Luo, M. F. *J. Phys. Chem. C* **2008**, *112*, 15045.
(21) Shapovalov, V.; Metiu, H. *J. Catal.* **2007**, *245*, 205.
(22) Reddy, B. M.; Thrimurthulu, G.; Katta, L.; Yamada, Y.; Park, S. E. *J. Phys. Chem. C* **2009**, *113*, 15882.
(23) Bueno-López, A.; Krishna, K.; Makkee, M.; Moulijn, J. A. *J. Catal.* **2005**, *230*, 237.
(24) Aneggi, E.; de Leitenburg, C.; Dolcetti, G.; Trovarelli, A. *Catal. Today* **2006**, *114*, 40.
(25) Liu, Z.; Zhou, R.; Zheng, X. *J. Nat. Gas Chem.* **2008**, *17*, 283.
(26) Liotta, L. F.; Ousmane, M.; Di Carlo, G.; Pantaleo, G.; Deganello, G.; Marcì, G.; Retailleau, L.; Giroir-Fendler, A. *Appl. Catal., A* **2008**, *347*, 81.
(27) Zhi, K.; Liu, Q.; Zhao, R.; He, R.; Zhang, L. *J. Rare Earths* **2008**, *26*, 538.
(28) Avgouropoulos, G.; Manzoli, M.; Boccuzzi, F.; Tabakova, T.; Papavasiliou, J.; Ioannides, T.; Idakiev, V. *J. Catal.* **2008**, *256*, 237.
(29) Ilieva, L.; Pantaleo, G.; Ivanov, I.; Nedyalkova, R.; Venezia, A. M.; Andreeva, D. *Catal. Today* **2008**, *139*, 168.
(30) Andreeva, D.; Ivanov, I.; Ilieva, L.; Abrashev, M. V.; Zanella, R.; Sobczak, J. W.; Lisowski, W.; Kantcheva, M.; Avdeev, G.; Petrov, K. *Appl. Catal., A* **2009**, *357*, 159.
(31) Penkova, A.; Charakova, C.; Laguna, O. H.; Hadjiivanov, K.; Romero-Sarria, F.; Centeno, M. A.; Odriozola, J. A. *Catal. Commun.* **2009**, *10*, 1196.
(32) Ilieva, L.; Pantaleo, G.; Ivanov, I.; Zanella, R.; Venezia, A. M.; Andreeva, D. *Int. J. Hydrogen Energy* **2009**, *34*, 6505.
(33) Zhang, C.; Michaelides, A.; King, D. A.; Jenkins, S. J. *J. Phys. Chem. C* **2009**, *113*, 6411.
(34) Zhang, C.; Michaelides, A.; King, D. A.; Jenkins, S. J. *Phys. Rev.* **2009**, *79*, 075433.
(35) Nolan, M. *J. Chem. Phys.* **2009**, *130*, 144702.
(36) Liu, Z. P.; Jenkins, S. J.; King, D. A. *Phys. Rev. Lett.* **2005**, *94*, 196102.
(37) Tabakova, T.; Boccuzzi, F.; Chiorino, A.; Manzoli, M.; Andreeva, D. *Appl. Catal., A* **2003**, *252*, 385.
(38) Ilieva, L.; Pantaleo, G.; Ivanov, I.; Venezia, A. M.; Andreeva, D. *Appl. Catal., B* **2006**, *65*, 101.
(39) Domínguez, M. I.; Sánchez, M.; Centeno, M. A.; Montes, M.; Odriozola, J. A. *Appl. Catal., A* **2006**, *302*, 96.
(40) Fu, Q.; Weber, A.; Flytzani-Stephanopoulos, M. *Catal. Lett.* **2001**, *77*, 87.
(41) Göpel, W.; Rocker, G.; Feierabend, R. *Phys. Rev. B* **1983**, *28*, 3427.
(42) Badri, A.; Binet, C.; Lavalley, J. C. *J. Chem. Soc., Faraday Trans.* **1996**, *92*, 4669.
(43) Fu, Q.; Saltsburg, H.; Flytzani-Stephanopoulos, M. *Science* **2003**, *301*, 935.

(44) Andreeva, D.; Tabakova, T.; Ilieva, L.; Naydenov, A.; Mehanjiev, D.; Abrashev, M. V. *Appl. Catal. A* **2001**, *209*, 291.
(45) Ilieva, L.; Sobczak, J. W.; Manzoli, M.; Su, B. L.; Andreeva, D. *Appl. Catal., A* **2005**, *291*, 85.
(46) Keramidas, V. G.; White, W. B. *J. Chem. Phys.* **1973**, *59*, 1561.
(47) Laguna, O. H.; Centeno, M. A.; Arzamendi, G.; Gandía, L. M.; Romero-Sarria, F.; Odriozola, J. A. *Catal. Today* **2009**, In press.
(48) Sanchez, M. G.; Gazquez, J. L. *J. Catal.* **1987**, *104*, 120.
(49) Pu, Z. Y.; Lu, J. Q.; Luo, M. F.; Xie, Y. L. *J. Phys. Chem. C* **2007**, *111*, 18695.
(50) Boccuzzi, F.; Chiorino, A.; Manzoli, M.; Andreeva, D.; Tabakova, T. *J. Catal.* **1999**, *188*, 176.
(51) Fronzi, M.; Piccinin, S.; Delley, B.; Traversa, E.; Stampfl, C. *Phys. Chem. Chem. Phys.* **2009**, *11*, 9188.
(52) Goguet, A.; Hardacre, C.; Harvey, I.; Narasimharao, K.; Saih, Y.; Sa, J. *J. Am. Chem. Soc.* **2009**, *131*, 6973.
(53) Lee, S.; Fan, C.; Wu, T.; Anderson, S. L. *J. Am. Chem. Soc.* **2004**, *126*, 5682.
(54) Rodriguez, J. A.; Wang, X.; Liu, P.; Wen, W.; Hanson, J. C.; Hrbek, J.; Pérez, M.; Evans, J. *Top. Catal.* **2007**, *44*, 73.
(55) Lee, S.; Fan, C.; Wu, T.; Anderson, S. L. *Surf. Sci.* **2005**, *578*, 5.
(56) Wörz, A. S.; Heiz, U.; Cinquini, F.; Pacchioni, G. *J. Phys. Chem. B* **2005**, *109*, 18418.
(57) Weststrate, C. J.; Westerström, R.; Lundgren, E.; Mikkelsen, A.; Andresen, J. N.; Resta, A. *J. Phys. Chem. C* **2009**, *113*, 724.
(58) Widmann, D.; Leppelt, R.; Behm, J. R. *J. Catal.* **2007**, *251*, 437.

JP1013225